要な役割を果たしている。関節が運動を行う際には，一方で運動が一定の範囲を超えないように制限され安定化の機構が働いている。関節包・靱帯・筋肉は安定化に寄与し，特に靱帯は関節包を補強するとともに，運動を一定の方向だけに制限し，過度の運動を防いで関節を安定化し保護する。このような骨関節のしくみのもと，関節は3次元運動として実に巧妙にさまざまな環境に適応的に働いていると言える。

骨関節の動態解析

整形外科領域における骨関節疾患は，動態の異常が原因となるケースが多く，これら疾患を治療する上で高精度な生体3次元骨関節動態を知ることが重要であると考えられている。しかしながら，これまで生体内における3次元動態解析は困難とされており，主に単純X線画像による2次元解析や屍体標本を用いた非生理的な解析がなされてきた。ここでは，肘関節を対象として，前節で述べた3D-3Dレジストレーション手法による3次元動態計測の例を示し，その解析結果について述べる。

肘関節の運動は，図11に示すように関節運動を4～5分割に静的な状態に分け，各肢位を3次元MRI装置で撮像することにより，連続的な時相の異なる3D画像として取得することができる。取得された画像に対して，各画像どうしをボクセル濃淡ベースレジストレーション（MRI画像における各骨要素のintensity（輝度値）はCT画像でいうCT値に相当する）することにより，画像内における3次元空間での位置・姿勢，すなわち3次元動態が求まる。また，得られた3次元動態データをコンピュータ上で視覚化・再現化し，さらに種々の定量データとして処理しやすい形にするため，輝度値情報をもつ3D画像から，骨要素内の骨表面のみを抽出した3次元骨表面形状モデルを作成する。ここでは，肘関節の3次元動態解析を，回転軸表記（スクリュー（螺旋）法）[20]を用いて行った結果の例を示す。

図12（下段）に示されるように，肘関節の屈伸運動は一軸性の回転運動ではなく，肘関節伸展位を基準とした各肢位間の回転軸は，上腕骨（肘関節）内側にある側副靭帯付着部に回転中心（回転軸の交点）が存在する多軸性の運動であることが分かる。また，図13は，前腕部での回内外運動（前腕を捻じる運動）におけるその回転軸が，手関節部に存在する尺骨頭の基部（Fovea;尺骨小窩）および肘関節部に存在する橈骨頭の中央部に集中し，比較的一軸性に近い運動であることを示している。

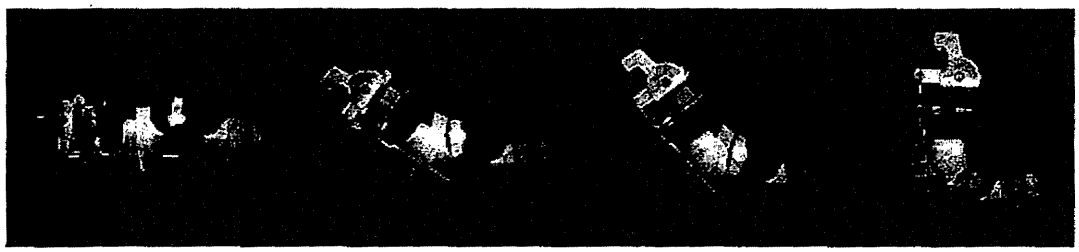

図11　肘関節の運動例
運動を4～5分割し，各肢位画像を3次元MRI装置にて取得する。

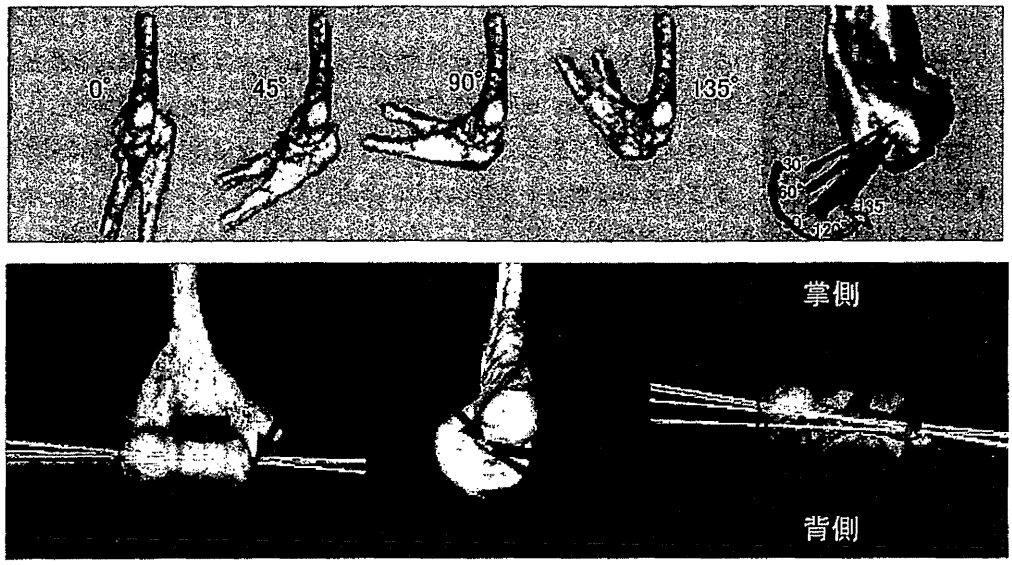

図 12　生体内3次元動態解析による肘関節屈伸運動（上段）とその屈伸運動における回転軸の動き（図の下段）
図は，肘関節部の屈伸運動は一軸性の回転運動ではなく，上腕骨（肘関節）内側にある側副靭帯付着部に回転中心（回転軸の交点）が存在する多軸性の運動であることを示す。

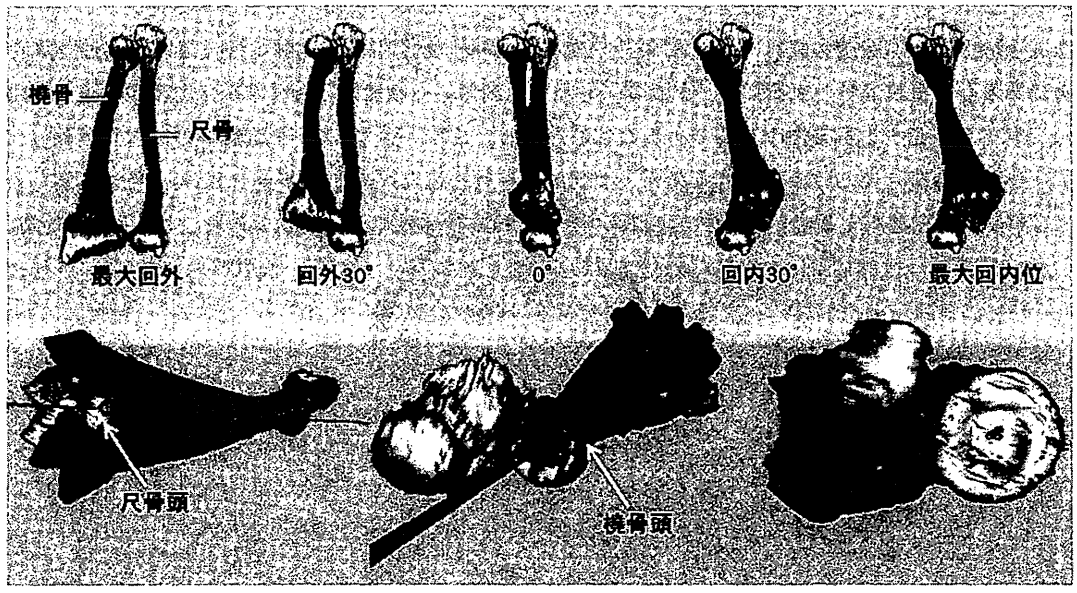

図 13　前腕回内外運動（前腕部を捻じる運動）
回転軸は手関節部に存在する尺骨頭の基部（Fovea;尺骨小窩）および肘関節部に存在する橈骨頭の中央部に集中し，比較的一軸性に近い運動であることを示す。

このように本例では静的な3次元動態解析であるものの，これまで行われてきた単純X線画像による2次元解析や屍体標本を用いた生理的筋緊張がない状態（非生体実験）での3次元動態解析法に比べて遥かに生理的かつ正確な動態解明ができるため，臨床的にも多くの知見が得られ，新しい治療戦略を立てる上でも大変有効であることが分かっている。また正常のみならず病的な動態の異常も容易に解析できるため，臨床応用が即期待でき，さらなる病態異常の原因追及等が可能になると考えられている。

骨関節の形態評価・術前計画シミュレーション

骨変形に対する矯正手術では医用画像を用いた術前評価，計画が重要である。しかしながら，従来の単純X線・CT画像を用いた2次元評価では，角状変形に回旋，短縮・延長を伴う3次元的に複雑な変形を正確に評価することは極めて困難である。にもかかわらず，過去の骨折変形治癒に対する変形解析の報告のほとんどが単純X線画像やCT断層画像を用いた評価法に基づいており，正確な3次元的定量解析が望まれている。以降では，肘関節を対象とした3D-3Dレジストレーション手法による形態評価・術前計画シミュレーションの手順例を取り上げ，その臨床的意義について述べる。

まず，対象となる肘関節の罹患骨全長および罹患骨に対応する健側骨全長のCT画像を撮影・取得し，骨表面のみを抽出した3次元骨表面形状モデルをそれぞれ作成する。次に，健側骨モデルから，患側に適合するように健側鏡像骨モデルを作成し，これを患側骨モデルに表面形状ベースレジストレーションによって重ね合わせる（図14左図）。具体的には，患側データの変形していない部分を基準側，変形している部分を変形側とし，健側データを患側データの基準側に重ね合わせ，その際の回転・移動マトリックス$M1$を得る。同様にして，健側データを患側データの変形部分にも重ね合わせ，回転・移動マトリックス$M2$を得る。以上から，健側データが患側まで変形する回転・移動マトリックスMは，

$$M = M2 \times M1^{-1}$$

と表すことができ，求められたMが罹患骨の3次元的変形量と見なすことができる（図14右図）。実際の患側の変形量は，近位側で重ね合わせた健側鏡像に基準軸を設定し，オイラー角によって6自由度評価を行うことになる。これら一連の手順によって，屈伸方向，内外反方向，回旋を含めた骨の回転・移動量を定量化でき，骨形態を含めた正確な術前計画シミュレーションが可能となる。以下では，実際の症例の解析結果を示す。

図15（上段）は，橈骨遠位端骨折における骨折変形治癒後のX線画像を示す。骨折変形治癒とは，骨折の転位が正確に整復・矯正されていない場合や，固定が不十分なために整復後転位が生じ，骨が変形を残したまま癒合したものを指す。本症例において，CT画像より両側橈骨3次元骨表面形状モデルを作成し，健側鏡像と患側骨モデルを近位で表面形状ベースレジストレーションによって重ね合わせた結果，健側と比較して橈屈8°，背屈25°，回旋11°の変形を認めた（図15の下段）。したがって，このシミュレーション結果によって得られた変形量を，実際の手術時に正確に再現すれば，健側鏡像とほぼ同一形態での整復が可能となる。ここでは，変形量を正確に再現する手術手技については触れ

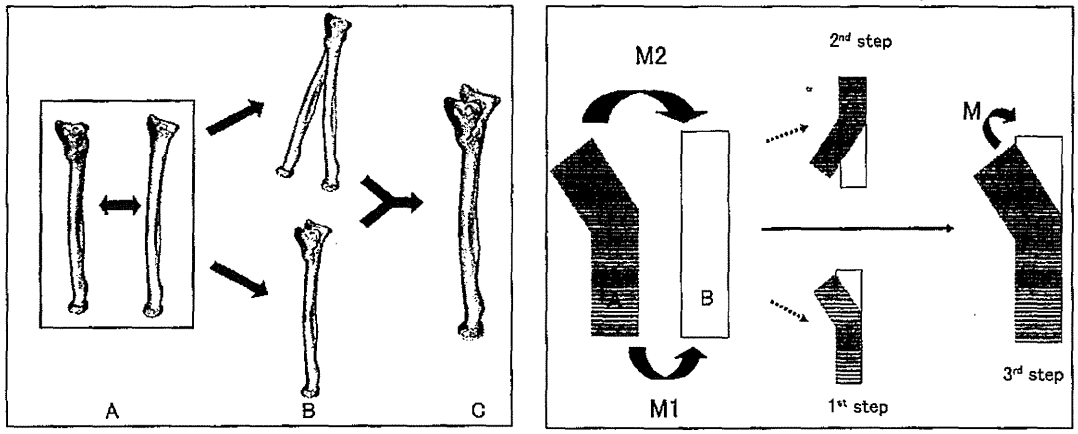

図 14　罹患骨モデル（黄色）と正常骨モデル（白）のレジストレーション（左図），およびその模式図（右図）
左図では，罹患骨モデル（黄色）と正常骨モデル（白）を比較し(A)，変形部の近位と遠位でレジストレーションを行うこと(B)で変形量を定量化する(C)。右図では，近位部分の移動マトリックスを M1，遠位部分の移動マトリックスを M2 とすれば，変形マトリックス M は，M2 と M1 の差分として計算される。（口絵 12）

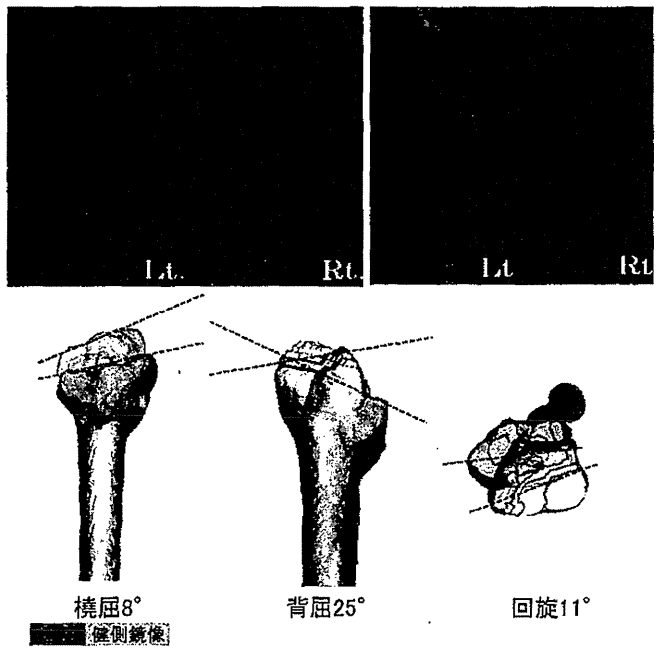

図 15　橈骨遠位端骨折における骨折変形治癒後の X 線画像（上段），および健側鏡像と患側骨モデルのレジストレーションによって得られた回転における変形量（下段）（口絵 13）

ないが，3 次元的な変形解析（形態評価・術前計画シミュレーション）が臨床的に非常に重要であることが十分推察されるであろう。

●5● おわりに ●●●

医工連携さらには産学連携による技術革新，産業創出が叫ばれて久しい。政府の支援を受けてさまざまなプロジェクトが立ち上げられてきたが，いわゆる成功例は数えるほどしかないのが現状である。本章の「医用画像による骨関節形態および動態解析・予測」は産業界で製作されるCTやMRI装置という診断機器が急速に進歩を遂げている一方で，医師サイドからは骨関節3次元動態を評価して治療したいというニーズは満足されていないという実情があったが，その間を工学系の情報，画像処理技術が埋めることによってすばらしい治療体系が広がろうとしている。そういう意味では本章内で紹介された技術は医工，産学連携の大成功例といえるだろう。また未来の治療への可能性を示唆するといった不確定なものではなく，すでにいくつかの医療施設では今週，来週の手術治療に用いられている。

しかるに，革新的な治療体系の門戸がようやく開かれたばかりであり，今後解決しなければならない問題点も山積している。しかし問題点に関しては，難破船が大海で進路がわからずに迷走するようなものではなく，問題点の方向性は明確である。それを多くの優秀な医・工・情報学系研究者が一つ一つ解決し，さらなる治療体系の革新に繋がることが望まれる。

今後高齢化社会のさらなる加速に伴ってニーズも加速度的に増大することが予想される。また骨関節のいわゆる整形外科領域だけでなく他の診療科でのニーズも汲んでいくことによって，研究領域も拡大していくものと思われる。さまざまな技術，研究を行っている医・工・情報学系研究者にとって，それが世の中でなんの役に立とうとしているかが，ややもすると曖昧になることがある。しかし悩める患者の治療に役立つという最も直接的な貢献を体感することは研究者冥利につきることである。多くの若手研究者が参画し，さまざまな分野で革新的な治療が広げられることを切望してやまない。

参考文献

(1) Lemieux, L *et al.* A patient-to-computed-tomography image registration method based on digitally reconstructed radiographs. *Med. Phys.* 21, 1749-1760 (1994)
(2) Murphy, MJ. An automatic six-degree-of-freedom image registration algorithm for image-guided frameless stereotaxic radiosurgery. *Med. Phys.* 24, 857-866 (1997)
(3) Weese J *et al.* Voxel-based 2-D/3-D registration of fluoroscopy images and CT scans for image-guided surgery. *IEEE Trans Inform. Technol. Biomed.* 1, 248-293 (1997)
(4) Hipwell JH. *et al.* Intensity-based 2-D－3-D registration of cerebral angiograms. *IEEE Trans. Med. Imag.* 22, 1417-1426 (2003)
(5) Banks, SA, Hodge, WA. Accurate measurement of three-dimensional knee replacement kinematics using single-plane fluoroscopy. *IEEE Trans. Biomed. Eng.* 43, 638-649 (1996)
(6) Hoff, WA. *et al.* Three-dimensional determination of femoral-tibial contact position under in-vivo conditions using fluoroscopy. *Clinical Biomech.* 13, 455-472 (1998)
(7) Zuffi, S. *et al.* A model-based method for the reconstruction of total knee replacement kinematics. *IEEE Trans. Med. Imag.* 18, 981-991 (1999)
(8) Mahfouz, MR. *et al.* A robust method for registration of three-dimensional knee implant models to two-

dimensional fluoroscopy images. *IEEE Trans. Med. Imag.* 22, 1561-1574 (2003)
(9) Yamazaki, T. *et al.* Improvement of depth position in 2-D/3-D registration of knee implants using single-plane fluoroscopy. *IEEE Trans. Med. Imag.* 23, 602-612 (2004)
(10) Weng, J. *et al.* Camera calibration with distortion models and accuracy evaluation. *IEEE Trans. Pattern. Anal. Mach. Intell.* 14, 965-980 (1992)
(11) Besl, PJ. and McKay, ND. A method for registration of 3-D shapes. *IEEE Trans. Pattern. Anal. Mach. Intell.* 14, 239-256 (1992)
(12) Lemieux, L. *et al.* Voxel based localization in frame-based and frameless stereotaxy and its accuracy. *Med. Phys.* 21, 1301-1310 (1994)
(13) Woods, RP. *et al.* MRI-PET registration with automated algorithm. *J. Comput. Assist. Tomogr.* 17, 536-546 (1993)
(14) Maes, F. *et al.* Multimodality image registration by maximization of mutual information. *IEEE Trans. Med. Imag.* 16,187-198 (1997)
(15) Holden, M. *et al.* Voxel similarity measures for 3-D serial MR brain image registration. IEEE Trans, Med. Imag. 19, 94-102 (2000)
(16) 松野誠夫ら『人工膝関節置換術―基礎と臨床―』文光堂，東京436-485 (2005)
(17) Tamaki M. *et al. In vivo* kinematic analysis of a high-flexion posterior stabilized fixed-bearing knee prosthesis in deep knee-bending motion. *J. Arthroplasty* 23, 879-885 (2008)
(18) Cates, HE. *et al. In vivo* comparison of knee kinematics for subjects having either a posterior stabilized or cruciate retaining high-flexion total knee arthroplasty. *J. Arthroplasty* 23, 1057-1067 (2008)
(19) Chouteau, J. *et al.* Kinematics of a cementless mobile bearing posterior cruciate ligament-retaining total knee arthroplasty. *Knee* 16, 223-227 (2009)
(20) Beggs, J. S. Kinematics. Washington: Hemisphere Publishing, 33-51 (1983)

Spine

SPINE Volume 36, Number 10, pp 778–783

BIOMECHANICS

In Vivo Three-Dimensional Kinematics of the Cervical Spine During Head Rotation in Patients With Cervical Spondylosis

Yukitaka Nagamoto, MD,* Takahiro Ishii, MD, PhD,† Hironobu Sakaura, MD, PhD,‡ Motoki Iwasaki, MD, PhD,‡ Hisao Moritomo, MD, PhD,‡ Masafumi Kashii, MD, PhD,§ Takako Hattori, MD,* Hideki Yoshikawa, MD, PhD,‡ and Kazuomi Sugamoto, MD, PhD*

Study Design. Kinematics of the cervical spine during head rotation was investigated using 3-dimensional (3D) magnetic resonance imaging (MRI) in patients with cervical spondylosis (CS).

Objective. To demonstrate *in vivo* 3D kinematics of the spondylotic cervical spine during head rotation.

Summary of Background Data. Several *in vivo* studies have identified kinematic differences between normal and spondylotic subjects, but only two-dimensional flexion/extension motion has been investigated. Differences of *in vivo* 3D cervical motion during head rotation between normal and spondylotic subjects have yet to be clarified.

Methods. Ten healthy volunteers (control group) and 15 patients with CS (CS group) underwent 3D MRI of the cervical spine with the head rotated to 5 positions (neutral, ±45° and ±maximal head rotation). Relative motions of the cervical spine were calculated by automatically superimposing a segmented 3D MRI of the vertebra in the neutral position over images for each position using volume registration. The 3D motions of adjacent vertebra were represented with 6 degrees of freedom by Euler angles and translations on the coordinate system.

Results. Compared with the control group, the CS group showed significantly decreased mean axial rotation and mean coupled lateral bending at C5–C6 and C6–C7 and significantly increased mean coupled lateral bending at C2–C3 and C3–C4, although both the groups showed the same pattern of coupled motions.

Conclusion. The *in vivo* 3D kinematics of the spondylotic cervical spine during head rotation was accurately depicted and compared with those of healthy cervical spines for the first time.

Key words: kinematics, coupled motion, cervical spondylosis, volume registration. **Spine 2011;36:778–783**

The human cervical spine is composed of highly specific tissues and structures, which together provide the extensive range of motion and considerable load-carrying capacity required for physical activities of daily living (ADL). This is 1 reason why degenerative changes in the cervical spine start as early as middle age and affect more than 95% of patients older than 65 years.[1] Even though nerve root or cord compression develops in 10% to 15% of the population,[2] the pathophysiology of cervical spondylosis (CS) remains poorly understood.[3]

Achieving a better understanding of this pathophysiology requires clarification of the differences in kinematics between the normal and spondylotic cervical spine. Several kinematic studies associated with aging and/or degeneration of the cervical spine have been reported using simple extension and flexion radiography,[4–7] motion analysis,[8] cineradiography,[9] and magnetic resonance imaging (MRI).[10] However, most of these studies have investigated only 2-dimensional flexion/extension motion, and 3-dimensional (3D) analysis using a motion analyzer has been vague and indirect. No study comparing in vivo 3D cervical motion during head rotation between normal and spondylotic subjects has been conducted, despite the importance of these motions in ADL. This is because of the difficulty in measuring *in vivo* cervical segmental motion, particularly during head rotation and lateral bending, which involves complex 3D motions called "coupled motion." We have developed a 3D MRI system to evaluate the *in vivo* 3D kinematics of the spine[11–14] and have already reported accurate *in vivo* 3D kinematics of the normal cervical spine using this method.[11–13] The objectives of this study were to investigate *in vivo* 3D kinematics of the spondylotic cervical spine during head rotation and to compare those with kinematics of the healthy cervical spine.

From the *Department of Orthopaedic Biomaterial Science Osaka University Graduate School of Medicine; †Department of Orthopaedic Surgery, Kaizuka City Hospital, Kaizuka; ‡Department of Orthopaedics, Osaka University Graduate School of Medicine; and §Department of Orthopaedic Surgery, Toyonaka Municipal Hospital, Shibahara, Toyonaka, Osaka, Japan.

Acknowledgment date: October 28, 2009. Revision date: March 13, 2009. Acceptance date: March 18, 2010.

The manuscript submitted does not contain information about medical device(s)/drug(s).

No funds were received in support of this work. No benefits in any form have been or will be received from a commercial party related directly or indirectly to the subject of this manuscript.

This study was approved by IRB of our institute.

Address correspondence and reprint requests to Yukitaka Nagamoto, MD, Department of Orthopaedic Biomaterial Science, Osaka University Graduate School of Medicine, 2-2 Yamadaoka, Suita, Osaka 5650871, Japan; E-mail: 7gam0to@gmail.com

DOI: 10.1097/BRS.0b013e3181e218cb

MATERIALS AND METHODS

Subjects in this study comprised 10 healthy volunteers (control group) and 15 patients with CS (CS group). The 10 healthy volunteers (5 men, 5 women; mean age, 25.1 years; range, 22–31 years) had neither neck pain nor any medical history of cervical spine disorders. As for the control group, all subjects were included in our previous publications[11–13] and retrospective analysis was performed. The 15 patients (7 men, 8 women; mean age, 60.2 years; range, 41–70 years) had been referred to our institution because of axial and/or neurologic symptoms and showed radiographic findings of CS as follows: loss of disc space height; spondylotic bars; foraminal osteophytes; and kyphosis. Subjects with a history of cervical spine surgery, trauma, tumors, infection, rheumatoid arthritis, or ossification of the posterior longitudinal ligament were excluded. All study protocols were approved in advance by the institutional review board.

Each subject was placed supine on the MRI table and underwent 3D MRI in 5 positions with the head rotated 0° (neutral position), 45°, and maximally to the left and right. All subjects were instructed to rotate the head as perpendicular as possible to the axis of the body trunk, and the shoulders were fixed to the table with a band. In the control group, MRI was performed using a 1.0-T commercial magnetic resonance system (Signa LX; General Electric, Milwaukee, WI). A 3D fast-gradient recalled acquisition in the steady state sequence was used with the following settings: repetition time, 8.0 ms; echo time, 3.3 ms; slice thickness, 1.5 mm; no interslice gap; flip angle, 10°; field of view, 24 cm; and 256 × 224 in-plane acquisition matrix. In the CS group, MRI was performed using a 1.5-T commercial magnetic resonance system (MAGNETOM Espree; Siemens, Erlangen, German). A 3D multiecho data imaging combination sequence was used with the following settings: repetition time, 40.0 ms; echo time, 20.0 ms; slice thickness, 1.3 mm; no interslice gap; flip angle, 12°; field of view, 24 cm; and 256 × 226 in-plane acquisition matrix. All subjects provided informed consent to undergo 3D MRI for the kinematics study and those for whom MRI proved difficult to perform because of axial and/or neurologic symptoms were excluded. All examinations were performed by the first or second author.

MRI data were saved in Digital Imaging and Communications in Medicine format and transmitted to a computer workstation, where image processing was performed using software developed in our laboratory (Virtual Place M series; Medical Imaging Laboratory, Tokyo, Japan). The method used in this study has been fully described in previous reports[11–13] and is, therefore, only described briefly here. This method showed high accuracy as follows: 0.24° for flexion/extension, 0.31° for lateral bending, 0.43° for axial rotation, 0.52 mm for superoinferior translation, 0.51 mm for anteroposterior translation, and 0.41 mm for lateral translation.[11] As a result of image processing (volume registration method), 3D motions of each vertebra expressed as a matrix were obtained. For easier comprehension of complicated 3D motions, relative 3D cervical motions of all motion segments were calculated by converting the matrix obtained by image processing into a matrix representing relative motion with respect to the inferior adjacent vertebra, and these motions were expressed in 6 degrees of freedom by Euler angles with the sequence of yaw (X)-pitch (Y)-roll (Z) and translations using a previously defined coordinate system as follows: the z-axis of occipital bone (Oc) was parallel to the line connecting anterior and posterior borders of the foramen magnum, with anterior considered positive. The y-axis was defined as perpendicular to the z-axis, with superior being positive. The x-axis was positive to the left. The coordinate system of C1 was defined using 2 points: the posteroinferior border of the anterior arch and the anteroinferior border of the posterior arch. Origins were located at the anterior border of the foramen magnum on Oc and the posteroinferior border of the anterior arch on C1. The coordinate system of subaxial cervical vertebrae was defined as follows: the origin was located at the most inferior point on the posterior wall of the vertebral body in the midsagittal plane. The z-axis was defined as the line connecting anterior and posterior points in the inferior plane of the vertebral body, with anterior considered positive. The y-axis was defined as perpendicular to the z-axis, with superior being positive. The positive x-axis was directed to the left (Figure 1).[11–13] The coordinate system was always set with moving vertebrae (suprajacent vertebra of the functional spinal unit) in this study. Mean values and standard

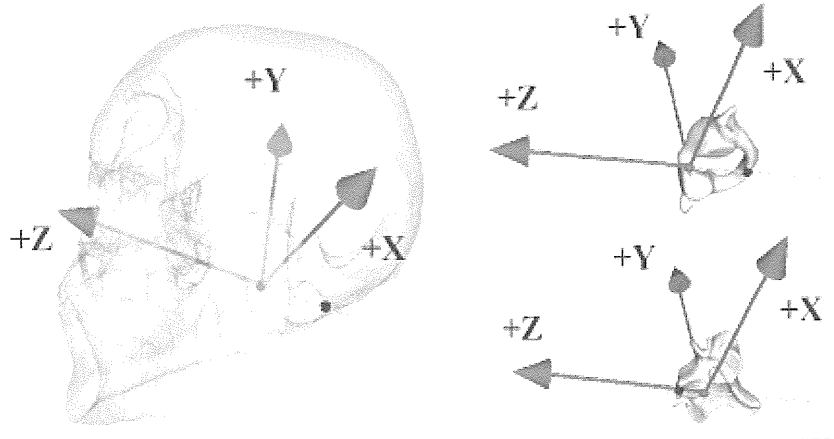

Figure 1. Anatomic orthogonal coordinate system for Oc, C1, and subaxial cervical vertebrae (C5). The methods have been fully described in previous studies.

TABLE 1. Rotations by Spinal Level for Control and CS Groups at 45° Head Rotation

	Oc–C1	C1–C2	C2–C3	C3–C4	C4–C5	C5–C6	C6–C7	C7–T1
AR								
Control(°)	0.4 ± 2.1	29.4 ± 3.2	0.5 ± 0.4	2.1 ± 0.5	2.4 ± 0.9	2.6 ± 0.7*	1.6 ± 0.7*	0.8 ± 0.6
CS(°)	0.2 ± 1.1	28.8 ± 3.7	0.9 ± 0.5	2.0 ± 0.7	2.0 ± 0.8	1.1 ± 0.7*	0.6 ± 0.3*	0.7 ± 0.3
Cp LB								
Control(°)	−4.0 ± 1.4*	−3.8 ± 1.8†	0.7 ± 1.2*	2.7 ± 0.7†	3.1 ± 0.8	2.8 ± 1.1*	2.5 ± 1.6†	0.5 ± 0.9
CS(°)	−2.3 ± 0.8*	−5.7 ± 1.6†	2.2 ± 1.0*	3.8 ± 1.2†	2.5 ± 1.3	1.3 ± 0.9*	1.3 ± 0.9†	0.6 ± 0.6
Cp F/E								
Control(°)	−5.4 ± 2.7†	−3.4 ± 2.0	−0.6 ± 1.0	0.8 ± 1.2	−1.1 ± 2.0	0.7 ± 1.5	1.0 ± 1.4†	0.8 ± 1.1
CS(°)	−7.7 ± 2.4†	−4.9 ± 2.8	−0.7 ± 0.4	−0.9 ± 0.7	−1.0 ± 1.1	−0.1 ± 0.7	0.5 ± 0.8†	1.3 ± 0.9

*$P < 0.01$.
†$P < 0.05$.
AR indicates axial rotation; Cp LB, coupled lateral bending; Cp F/E, coupled flexion/extension; CS, cervical spondylosis.

deviations for range of motion to 1 side were computed in each group. Segmental motions were calculated as the average of the sum between left and right motions for coupled extension flexion, coupled anteroposterior translation, and coupled superoinferior translation, using constant codes between left and right rotation, and also calculated as the average difference between left and light motions for main axial rotation, coupled lateral bending, and lateral translation, using differing codes between left and right rotation.

In addition, degree of head rotation was measured accurately on the absolute spatial coordinate system using volume registration of the occiput. A 3D animation of each subject was also constructed to facilitate an understanding of these complex motions using methods that have been fully described in previous studies.[11–13]

Comparisons of rotations and translations by spinal level between groups were performed using the nonparametric Mann-Whitney *U* test. Values of $P < 0.05$ were considered statistically significant.

RESULTS

Mean (±standard deviation) maximal head rotation was 72.0 ± 5.3° in the control group and 63.4 ± 8.9° in the CS group. As a large range of mobility was identified between groups, only kinematics at 45° of head rotation was compared.

Main Axial Rotation at 45° Head Rotation

Significant decreases in axial rotation were observed at C5–C6 and C6–C7 in the CS group at both 45° (Table 1 and Figure 2).

Coupled Lateral Bending at 45° Head Rotation

In both groups, coupled lateral bending opposite to head rotation to 1 side was observed in the upper cervical spine, whereas the subaxial cervical spine displayed coupled lateral bending in the same direction as head rotation (Table 1 and Figure 3). Significant decreases in coupled lateral bending were observed at Oc–C1, C5–C6, and C6–C7, and significant increases were also observed at C1–C2, C2–C3, and C3–C4 in the CS group compared with the control group.

Coupled Flexion/Extension at 45° Head Rotation

In both groups, extension coupled with head rotation to 1 side occurred in the upper and middle cervical spine, whereas in the lower cervical spine, flexion was coupled with head rotation (Table 1 and Figure 4). Significant decreases in coupled flexion/extension were observed at C6–C7, and significant increases were observed at Oc–C1 in the CS group compared with the control group.

Coupled Translations at 45° Head Rotation

Although coupled translations were barely seen and most of these values were beyond the limit of accuracy and too small to analyze statistically, concerning lateral translation, the CS group showed a tendency toward larger motion in the middle

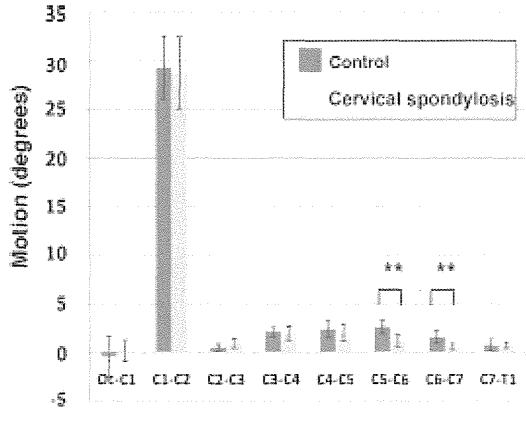

Figure 2. Main axial rotation by spinal level for the Control and CS groups at 45° head rotation. Data represent mean ± standard deviation. *$P < 0.05$ and **$P < 0.01$.

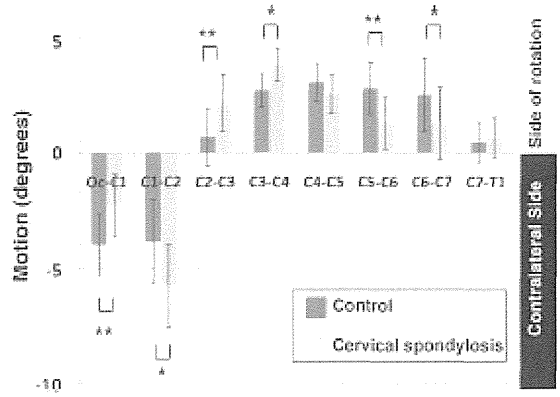

Figure 3. Coupled lateral bending by spinal level for the Control and CS groups at 45° head rotation. Data represent mean ± standard deviation. $^{*}P < 0.05$ and $^{**}P < 0.01$.

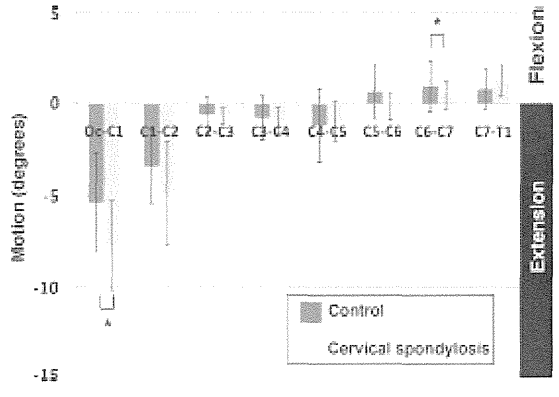

Figure 4. Coupled flexion/extension by spinal level for the Control and CS groups at 45° head rotation. Data represent mean ± standard deviation. $^{*}P < 0.05$ and $^{**}P < 0.01$.

cervical spine compared with the control group (Table 2 and Figure 5).

DISCUSSION

Hypomobility at the Lower Cervical Segments in the Degenerative Cervical Spine

General agreement is seen in the literature that the most commonly involved level is at C5–C6, followed by C6–C7 with increasing age.[4,15,16] Degenerative changes are speculated to arise most frequently at these levels because maximum distribution of axial load occurs at the lower cervical levels representing the sites of lordotic inversion.[10,17,18] To the best of our knowledge, few studies have addressed the *in vivo* kinematic changes of cervical motion segments after degeneration, despite a number of 2-dimensional flexion/extension motion studies of the normal cervical spine. Dvorak *et al*[4] showed significant hypomobility in sagittal rotation at C6–C7 in subjects with degenerative spine based on a functional flexion/extension radiographic study. Miyazaki *et al*[10] revealed that decreased segmental motion during extension-flexion starts at C4–C5 and C5–C6 with increasing age in a kinetic MRI study. No studies have clarified the kinematic changes occurring head rotation, because of the difficulties inherent in measuring such 3D motions *in vivo*. This study succeeded in detecting kinematics of the cervical spine during head rotation in patients with CS using a unique method. Comparison with healthy cervical spines yielded comparable results to previous cervical flexion/extension motion studies, showing significant decreases in main axial rotation and coupled lateral bending during headrotation at C5–C6 and C6–C7 segments in the CS group. These results indicate that in the lower cervical spine of the CS group, which is vulnerable to degeneration, motion segments might have already been in the stabilization phase put forward by Kirkaldy-Willis and Farfan[19] and hypomobility might have been present.

As for main axial motion, significant compensatory motions were barely seen at the suprajacent segments. However, the question arises as to where compensation occurs, because both groups were compared at 45° fixed head rotation. Total cervical motion at 45° fixed head rotation and the

TABLE 2. Coupled Translations by Spinal Level for Control and CS Groups at 45° Head Rotation

	C2–C3	C3–C4	C4–C5	C5–C6	C6–C7	C7–T1
Lateral translation						
Control (mm)	0.2 ± 0.0	−0.2 ± 0.0	−0.4 ± 0.1	−0.5 ± 0.0	−0.3 ± 0.1	−0.2 ± 0.0
CS (mm)	−0.2 ± 0.2	−0.6 ± 0.3	−0.5 ± 0.2	−0.5 ± 0.4	−0.3 ± 0.1	−0.2 ± 0.0
Superoinferior translation						
Control (mm)	−0.1 ± 0.1	−0.1 ± 0.2	−0.0 ± 0.3	0.1 ± 0.3	0.3 ± 0.3	0.2 ± 0.5
CS (mm)	−0.2 ± 0.1	−0.1 ± 0.2	−0.1 ± 0.1	−0.0 ± 0.1	0.1 ± 0.2	0.1 ± 0.2
Anteroposterior translation						
Control (mm)	−0.1 ± 0.2	−0.1 ± 0.2	−0.0 ± 0.3	0.2 ± 0.3	0.4 ± 0.4	0.3 ± 0.7
CS (mm)	−0.1 ± 0.1	−0.1 ± 0.2	−0.1 ± 0.2	0.1 ± 0.1	0.1 ± 0.1	0.2 ± 0.1

CS indicates cervical spondylosis.

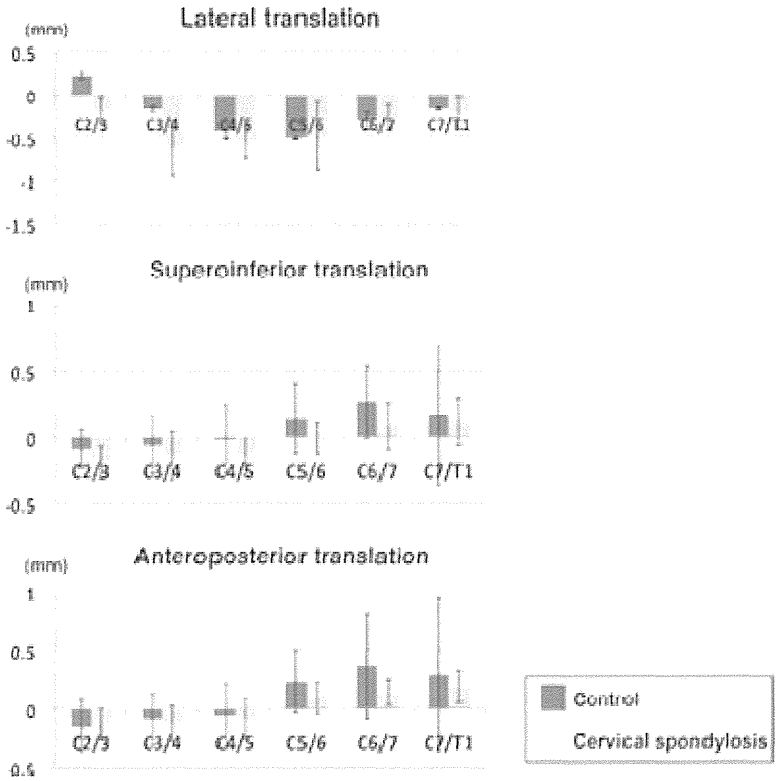

Figure 5. Coupled translations by spinal level for the Control and CS groups at 45°. Intervertebral motions are expressed in mm.

contribution ratio ([total cervical rotation [°]/head rotation [°]] × 100) was 38.9° (89%) in the control group and 36.4° (83%) in the CS group. Slight but significant decreases in motion were identified in the CS group ($P < 0.01$, nonparametric Mann-Whitney *U* test). Given the above findings, some compensation can safely be said to occur beyond the upper thoracic spine, but the precise location at which compensation occurred could not be identified.

Coupling Pattern of the Degenerative Cervical Spine

Although coupling patterns provide important clues for the detection of selected elements of spine pathology,[20] coupled motion is thought to be difficult to assess precisely because of the complex 3D motions and *in vivo* explorations have been rare. White and Panjabi[21] described abnormal coupled motion as 1 feature of abnormal spine kinematics. As we have already succeeded in accurately detecting 3D coupled motion of the cervical spine *in vivo*, we investigated coupled patterns of the spondylotic cervical spine during head rotation and compared the results with those of the healthy cervical spine. Although almost the same coupling patterns were identified in both groups, the spondylotic cervical spine showed significant hypomobility in axial and lateral directions at the lower cervical spine and significant lateral hypermobility, including coupled lateral bending at the middle cervical spine (Table 3). The fact that hypermobility in lateral directions was observed at the middle cervical spine in the CS group compared with the control group indicates that intervertebral mechanical stresses are increased in lateral directions at the middle cervical spine. As head axial rotation movements are reportedly half as frequent as flexion/extension movements and just as frequent as lateral bending movements,[22] head axial rotation movements are often repeated during ADL. Given these considerations, repetition of head rotation in ADL might have promoted degenerative changes of the middle cervical spine in the CS group.

This study has several limitations. First, the information was not obtained from true real-time imaging in the upright position. Second, the study was conducted using a small sample size. Third, patients were grouped together in the CS group despite a wide degree of variation in age, deformity, and symptoms. In this regard, further research focused more specifically on a particular subject group should be undertaken to elucidate details of the natural history of cervical

TABLE 3. Summary of Coupling Pattern for the CS Group Compared With the Control Group

	Main Motion	Coupled LB	Coupled F/E
Upper (Oc–C2)	N	N	N
Middle (C2–C5)	N	Increased	N
Lower (C5–T1)	Decreased	Decreased	N

LB indicates lateral bending; F/E, flexion/extention; N, no marked difference between groups; CS, cervical spondylosis.

spine motion after degeneration. Fourth, there might be some differences between the images obtained from the 2 different scanners in the 2 groups. Despite all these limitations, no other approaches to kinematic analysis have provided the kind of information given in this study, and these findings thus represent a step toward a better understanding of CS.

In conclusion, we accurately determined *in vivo* 3D kinematics of the spondylotic cervical spine during head rotation and compared the results with kinematics for the healthy cervical spine for the first time. Comparison with healthy cervical spine yielded comparable results with previous cervical flexion/extension motion studies, significant decreases in main axial rotation, and coupled lateral bending during head rotation at C5–C6 and C6–C7 segments in the spondylotic cervical spine. Although almost the same coupling patterns were observed in both groups, significant hypomobility in axial and lateral directions at the lower cervical spine and significant hypermobility in lateral directions at the middle cervical spine were apparent in the spondylotic cervical spine. Because hypermobility in lateral directions at the middle cervical spine in the CS group were thought to reflect increased intervertebral mechanical stresses, repeated head rotation in ADL might contribute to the progression of degenerative changes in the middle cervical vertebrae of the spondylotic cervical spine.

Key Points

- *In vivo* 3D kinematics of the spondylotic cervical spine during head rotation was investigated for the first time.
- Almost the same coupling patterns were observed in both healthy and spondylotic cervical spine.
- Significant hypomobility at the lower cervical segments were observed in the spondylotic cervical spine; significant decreases in main axial rotation and coupled lateral bending at C5–C6 and in coupled flexion/extension as well as main axial rotation and coupled lateral bending at C6–C7.
- On the contrary, significant hypermobility in lateral directions were observed at the middle cervical segments in the spondylotic cervical spine; significant increases in coupled lateral bending at C2–C3 and C3–C4.

Acknowledgments

The authors thank Ryoji Nakao and Aya Sasaki for assisting with software programming and Yoshihiro Sakaguchi for help with magnetic resonance imaging.

References

1. Garfin SR. Cervical degenerative disorders: etiology, presentation, and imaging studies. *Instr Course Lect* 2000;49:335–8.
2. Kolstad F, Myhr G, Kvistad KA, et al. Degeneration and height of cervical discs classified from MRI compared with precise height measurements from radiographs. *Eur J Radiol* 2005;55:415–20.
3. Muhle C, Metzner J, Weinert D, et al. Classification system based on kinematic MR imaging in cervical spondylitic myelopathy. *AJNR Am J Neuroradiol* 1998;19:1763–71.
4. Dvorak J, Panjabi M, Grob D, et al. Clinical validation of functional flexion/extension radiographs of the cervical spine. *Spine* 1993;18:120–7.
5. Holmes A, Wang C, Han ZH, et al. The range and nature of flexion-extension motion in the cervical spine. *Spine* 1994;19:2505–10.
6. Dai L. Disc degeneration and cervical instability. Correlation of magnetic resonance imaging with radiography. *Spine* 1998;23:1734–8.
7. Lind B, Sihlbom H, Nordwall A, et al. Normal range of motion of the cervical spine. *Arch Phys Med Rehabil* 1989;70:692–5.
8. Dvorak J, Antinnes JA, Panjabi M, et al. Age and gender related normal motion of the cervical spine. *Spine* 1992;17:S393–8.
9. Cheng JS, Liu F, Komistek RD, et al. Comparison of cervical spine kinematics using a fluoroscopic model for adjacent segment degeneration. Invited submission from the Joint Section on Disorders of the Spine and Peripheral Nerves, March 2007. *J Neurosurg Spine* 2007;7:509–13.
10. Miyazaki M, Hong SW, Yoon SH, et al. Kinematic analysis of the relationship between the grade of disc degeneration and motion unit of the cervical spine. *Spine* 2008;33:187–93.
11. Ishii T, Mukai Y, Hosono N, et al. Kinematics of the upper cervical spine in rotation: *in vivo* three-dimensional analysis. *Spine* 2004;29:E139–44.
12. Ishii T, Mukai Y, Hosono N, et al. Kinematics of the subaxial cervical spine in rotation *in vivo* three-dimensional analysis. *Spine* 2004;29:2826–31.
13. Ishii T, Mukai Y, Hosono N, et al. Kinematics of the cervical spine in lateral bending: *in vivo* three-dimensional analysis. *Spine* 2006;31:155–60.
14. Fujii R, Sakaura H, Mukai Y, et al. Kinematics of the lumbar spine in trunk rotation: *in vivo* three-dimensional analysis using magnetic resonance imaging. *Eur Spine J* 2007;16:1867–74.
15. Shedid D, Benzel EC. Cervical spondylosis anatomy: pathophysiology and biomechanics. *Neurosurgery* 2007;60:S7–13.
16. Friedenberg ZB, Edelken J, Spencer HN, et al. Degenerative changes in the cervical spine. *J Bone Joint Surg Am* 1959;41:61–70.
17. Gallucci M, Limbucci N, Paonessa A, et al. Degenerative disease of the spine. *Neuroimaging Clin N Am* 2007;17:87–103.
18. Jager HJ, Gordon-Haris I., Mehring UM, et al. Degenerative change in the cervical spine and load-carrying on the head. *Skeletal Radiol* 1997;26: 475– 81.
19. Kirkaldy-Willis WH, Farfan HF. Instability of the lumbar spine. *Clin Orthop Relat Res* 1982;(165):110–23.
20. Cook C, Heqedus E, Showalter C, et al. Coupling behavior of the cervical spine: a systematic review of the literature. *J Manipulative Physiol Ther* 2006;29:570–5.
21. White AA, Panjabi MM. *Clinical Biomechanics of the Spine*. 2nd ed. Philadelphia, PA: Lippincott Williams & Wilkins; 1990.
22. Sterling AC, Cobian DG, Anderson PA, et al. Annual frequency and magnitude of neck motion in healthy individuals. *Spine* 2008;33:1882–8.

Eur Spine J (2011) 20:1745–1750
DOI 10.1007/s00586-011-1869-4

ORIGINAL ARTICLE

In vivo three-dimensional segmental analysis of adolescent idiopathic scoliosis

Takako Hattori · Hironobu Sakaura · Motoki Iwasaki · Yukitaka Nagamoto · Hideki Yoshikawa · Kazuomi Sugamoto

Received: 9 August 2010 / Revised: 16 April 2011 / Accepted: 29 May 2011 / Published online: 18 June 2011

Abstract
Introduction An accurate assessment of three-dimensional (3D) intervertebral deviation is crucial to the better surgical correction of adolescent idiopathic scoliosis (AIS). However, a precise 3D study of intervertebral deviation has not been previously reported.
Objective The purpose of the present study is to evaluate the intervertebral coronal inclination, axial rotation and sagittal angulation of AIS using 3D bone models and a local coordinate system.
Materials and methods 3D bone models of the thoracic and lumbar spine of ten AIS patients were constructed using computed tomography. The local coordinate axis was determined semi-automatically for each vertebra. By using these local coordinates, the intervertebral deviation angles were calculated in the coronal, axial and sagittal planes and projected to subjacent local coordinates.
Result The intervertebral deformity in the coronal plane was larger near the apical region and smaller near the junctional region. Conversely, the intervertebral rotation in the axial plane was smaller near the apical region, and larger near the junctional region. Concerning the sagittal plane deformity, the constant tendency was not recognized.
Conclusion Using a local coordinate system for the vertebra of AIS, we measured the 3D intervertebral coronal, axial and sagittal deviation of the thoracolumbar spine and found that the change in the intervertebral inclination angle in the coronal plane increased toward the apical region and decreased toward the junctional region, and that the converse tendency was noted for the axial intervertebral rotational angle. This analysis provides an improved 3D guide for the surgical correction of AIS.

Keywords Idiopathic scoliosis · Three-dimensional · Intervertebral deviation · Local coordinate system

T. Hattori (✉) · Y. Nagamoto · K. Sugamoto
Division of Orthopaedic Biomaterial Science, Osaka University Graduate School of Medicine, 2-2, Yamadaoka, Suita, Osaka 565-0871, Japan
e-mail: takako-hattori@umin.ac.jp

H. Sakaura · M. Iwasaki · H. Yoshikawa
Department of Orthopaedics, Osaka University Graduate School of Medicine, 2-2, Yamadaoka, Suita, Osaka 565-0871, Japan

Introduction

Adolescent idiopathic scoliosis (AIS) is a three-dimensional (3D) deformity associated with lateral deviation in the coronal plane, thoracic hypokyphosis in the sagittal plane and rotation in the axial plane [3, 4, 25]. However, two-dimensional evaluation of AIS remains the mainstay of most studies of AIS [10, 18]. In 2008, Modi et al. [18] reported the wedging angle of both the vertebral body and intervertebral disc and correlated the apical wedging angle and the severity of the curve in 150 AIS patients using only anteroposterior radiographs in the standing position. For evaluation in the transverse plane, Kotwicki et al. [10] used only a single axial slice from a computed tomography (CT) scan at the apex to measure the rotational angle and the intravertebral deformation. The asymmetry in the shape of the vertebral body and spinal canal and rotational deformity in the axial plane in AIS patients further contribute to the inaccuracy of such assessments of the vertebral axis in the two-dimensional plane.

3D evaluation of AIS is also gaining popularity. The in vitro 3D reconstruction of cadaveric vertebrae using 3D morphometric analysis [21–23], such as vertebral wedging, pedicle width, pedicle length, pedicle height, pedicle

inclination and facet surface, is a recent example. In addition, several studies concerning 3D reconstruction of the spine using biplane radiographic images have been reported [2, 8, 9]. The method proposed by Kadoury et al. enabled 3D reconstruction from biplane radiographs. Although their studies involve 3D analysis of an in vivo model, their reconstructed bone models used anthropometric data and not patients' bones.

An accurate assessment of 3D intervertebral deviation is crucial to the better surgical correction of the deformity. Although there have been some studies regarding intervertebral deviation of AIS [5, 7, 24], no detailed 3D study using an in vivo model of AIS has been reported. Therefore, the present study aimed to develop a local coordinate system for the AIS vertebra and to evaluate the in vivo 3D intervertebral deviation in the coronal, axial and sagittal planes in order to provide guidance for its surgical correction.

Materials and methods

Patients

We examined spinal CT images from consecutive ten patients with AIS who were scheduled for corrective surgery. The patients included two males and eight females, with an age range of 12 to 19 years (mean 14.7 years) at the time of operation. Before CT imaging, anteroposterior (AP) plain radiographs were taken in the upright position. On AP radiographs, the measured mean Cobb's angles were 62.5° (range 29°–77°) at the thoracic curvature and 50.3° (range 30°–73°) at the lumbar curvature. According to King's classification [11], the curves were type I in two patients, type II in one, type III in six and type IV in one. Risser sign [15] showed grade 0 in two, grade 3 in four, and grade 4 in four patients. Nash and Moe's vertebral rotation [19] of the apex showed grade + in one, grade ++ in seven, and grade +++ in two patients.

The protocol was approved by the institutional boards of the hospital and fully informed consent was obtained from all participants.

CT image acquisition

Prior to surgery, all ten patients underwent CT scans of the entire deformed spine in the supine position. Scans were performed using a helical CT scanner (Light Speed VCT, General Electric, Maukesha, WI). The slice thickness was 0.625 mm, the tube voltage was 120 kV and the amperage was 90 mA. The data were saved in a standard DICOM (Digital Imaging and Communications in Medicine) format. The estimated radiation dose for the patients using this scanning protocol was 5.2 mSv.

Construction of 3D surface bone models

To construct the 3D bone models, we performed a segmentation procedure. Segmentation extracts bone regions and associates each region with individual bones. The anatomic structure or region of interest must be delineated and separated so that it can be viewed individually. Regions of individual bones were segmented semiautomatically using a software program for image analysis (Virtual Place-M; AZE Ltd, Tokyo, Japan). We then obtained the surface models of the vertebrae by applying 3D surface generation of the bone cortex [18, 20].

Axis configuration of local anatomic coordinate system

In order to measure the deviation in three dimensions between adjacent vertebrae, we first established the axis of the local coordinate system for each vertebra by first calculating the centroid of the vertebra automatically and designating it as the origin of the coordinate axis (Fig. 1a). Next, the planar approximation of the superior endplate was calculated using the least-squares method and we estimated a plane parallel to the superior endplate via the origin (Fig. 1b). On that plane, a line from both the centroid and the point which divided the front part of the vertebral body into half (using the least-squares method) formed the z axis (Fig. 1c), with 'anterior' as the 'positive' direction. A line perpendicular to the z axis pointing to the left formed the x axis. Finally, the y axis was defined as a line perpendicular z–x plane (Fig. 1d).

Measurement of intervertebral coronal plane deformity

The intervertebral coronal inclination between adjacent vertebrae was defined as the angle between adjacent x axes projected on the subjacent local coordinate x–y plane. From T1–T2 to L4–L5, each intervertebral coronal inclination was measured. For example, the adjacent inclination in the coronal plane of T8–T9 represented the angle between x axes of T8 and T9 projected to the x–y plane of T9 (Fig. 2). All adjacent intervertebral angles were measured automatically.

Measurement of intervertebral axial plane deformity

The intervertebral rotation in the axial plane between adjacent vertebrae was defined as the angle between adjacent z axes projected on the subjacent local coordinate z–x plane. From T1–T2 to L4–L5, each intervertebral axial rotation angle was measured. For example, the adjacent rotation in the axial plane of T8–T9 represented the angle between z axes of T8 and T9 projected to the z–x plane of

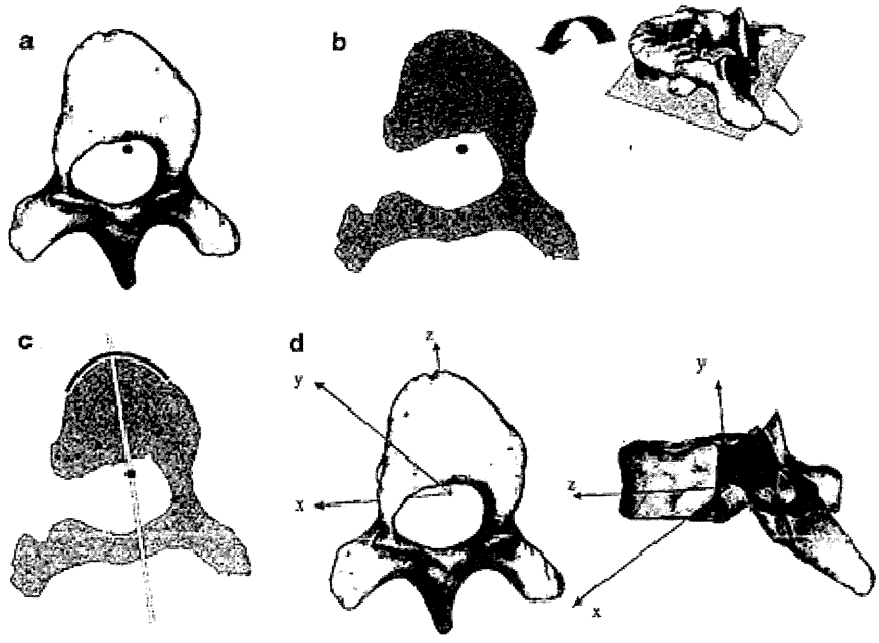

Fig. 1 The method used to establish the local coordinate system. **a** The *black sphere* is a centroid of the vertebra that is defined as the origin of the coordinate axis. **b** The cross-sectional surface of the vertebra; the planar approximation of the superior endplate was calculated using the least-squares method, and we estimated a plane parallel to the superior endplate via the origin. **c** In the cross-sectional plane, the *z* axis is defined as a line between the centroid and the point that divides the front portion of the vertebral body in half. **d** A line perpendicular to the *z* axis and pointing to the left on the plane forms the *x* axis. Finally, the *y* axis pointing cranial is defined as a line perpendicular to the *z*–*x* plane

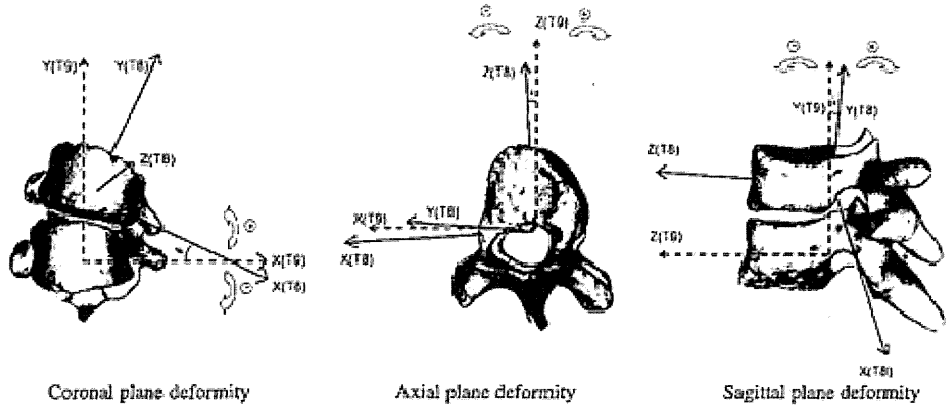

Coronal plane deformity Axial plane deformity Sagittal plane deformity

Fig. 2 The T8 and T9 bone models and each local coordinate axis. The *solid lines* present the axis of T8, and the *broken lines* present the axis of T9. *Left* the intervertebral coronal inclination. The figure faces the subjacent vertebral *x*–*y* plane; the intervertebral coronal inclination angle (*arrow*) is defined as the angle between two adjacent *x* axes projected on the subjacent *x*–*y* plane. *Middle* the intervertebral axial rotation. The figure faces the subjacent *z*–*x* plane; the intervertebral axial rotational angle (*arrow*) is defined as the angle between adjacent *z* axes projected on the subjacent *z*–*x* plane. *Right* the intervertebral sagittal angulation. The figure faces the subjacent *y*–*z* plane; the sagittal intervertebral angulation (*arrow*) is defined as the angle between adjacent *y* axes projected on the subjacent *y*–*z* plane

T9 (Fig. 2). All adjacent intervertebral angles were also measured automatically.

Measurement of intervertebral sagittal plane deformity

The intervertebral angulation in the sagittal plane between adjacent vertebrae was defined as the angle between adjacent *y* axes projected on the subjacent local coordinate *y*–*z* plane. From T1–T2 to L4–L5, each intervertebral sagittal angulation was measured. For example, the adjacent angulation in the sagittal plane of T8–T9 represented the angle between *y* axes of T8 and T9 projected to the *y*–*z* plane of T9 (Fig. 2). All adjacent intervertebral angles were also measured automatically.

Results

Intervertebral coronal plane deformity

The left side of Fig. 3 shows the amount of change between each intervertebral coronal inclination for all ten patients. These results indicate that the intervertebral deformity in the coronal plane was larger near the apical region and

smaller near the junctional region. The maximum intervertebral change at apical region was 20.2° (absolute value), the minimum change at junctional region was 0°. Figure 4 shows two representative cases (Case 3 and Case 10). The 3D models of both the thoracic and lumbar spine and the intervertebral angle in the coronal and axial planes are shown in Fig. 4. The *x* axis of the graph to the left of the bone model represents the intervertebral inclination angle in the coronal plane. The 'plus' direction of the graph means that the *x* axis of the suprajacent vertebra is directed in the 'plus' direction in relation to the subjacent vertebral *y* axis. Similarly, the minus direction of the graph means that the adjacent vertebral *x* axis is directed in the minus direction in relation to the *y* axis of the subjacent vertebra (Fig. 2).

Intervertebral axial plane deformity

The middle of Fig. 3 shows the amount of change between each intervertebral axial rotation for all patients. As the converse to the intervertebral coronal deformity, the intervertebral rotation in the axial plane was smaller near the apical region and larger near the junctional region. The maximum intervertebral change at junctional region was 12.6° (absolute value), the minimum change at apical region was 0°. The angle to the plus direction represents the amount of axial rotational change in the clockwise rotation of the suprajacent vertebra to subjacent *z*–*x* plane. On the other hand, when the suprajacent vertebral body rotates to the counterclockwise for the subjacent vertebral body, the change in the angle of the adjacent vertebral body is directed in the minus direction (Fig. 2). The amount of changes between adjacent vertebral axial rotation of two representative cases (Case 3 and Case 10) are shown in the graphs to the right of the bone models (Fig. 4).

Intervertebral sagittal plane deformity

The right side of Fig. 3 shows the amount of change between each intervertebral sagittal angulation for all the patients. Concerning the sagittal plane deformity, the constant tendency was not recognized. The 'plus' represents that the *y* axis of the suprajacent vertebra is directed in the minus direction in relation to the subjacent vertebral *z* axis. It means that the suprajacent vertebral bodies located in extension to subjacent vertebral bodies on subjacent *y*–*z* planes (Fig. 2).

Discussion

Idiopathic scoliosis is a complex spinal deformity characterized by lateral curvature of the spine associated with axial vertebral rotation. Recent 3D evaluations of the spine

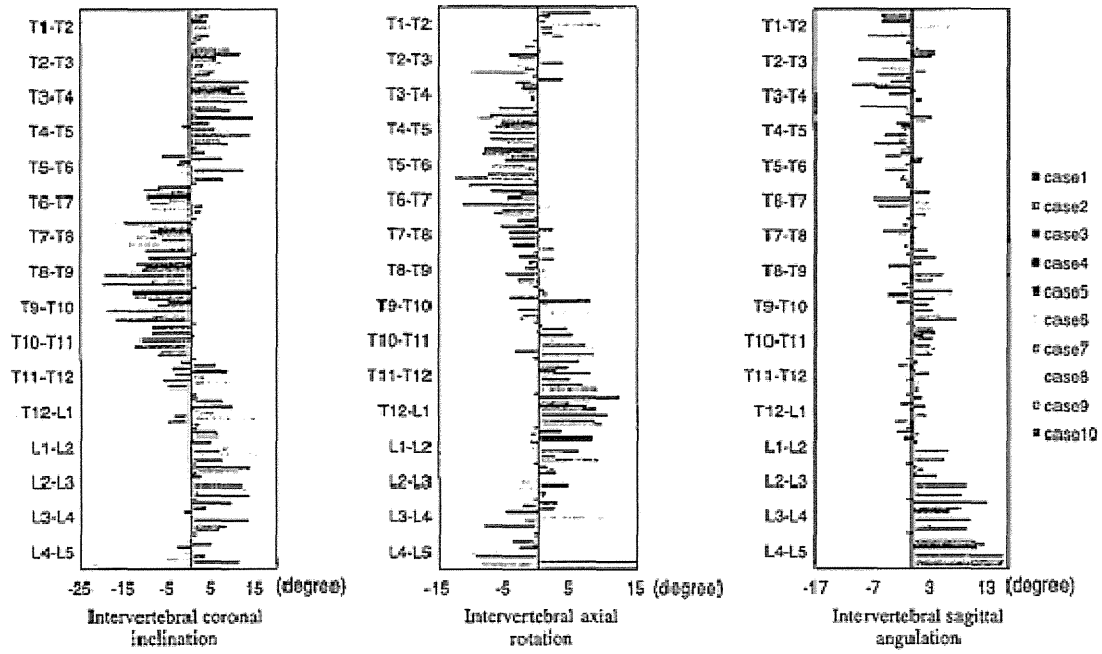

Fig. 3 The intervertebral deviation of the each adjacent vertebrae of all ten patients. The *x* axes show the each intervertebral deviation angles of all patients in coronal, axial and sagittal plane. The intervertebral deformity in the coronal plane was larger near the apical region and smaller near the junctional region. Conversely, the intervertebral rotation in the axial plane was smaller near the apical region, and larger near the junctional region. Concerning the sagittal plane deformity, the constant tendency was not recognized

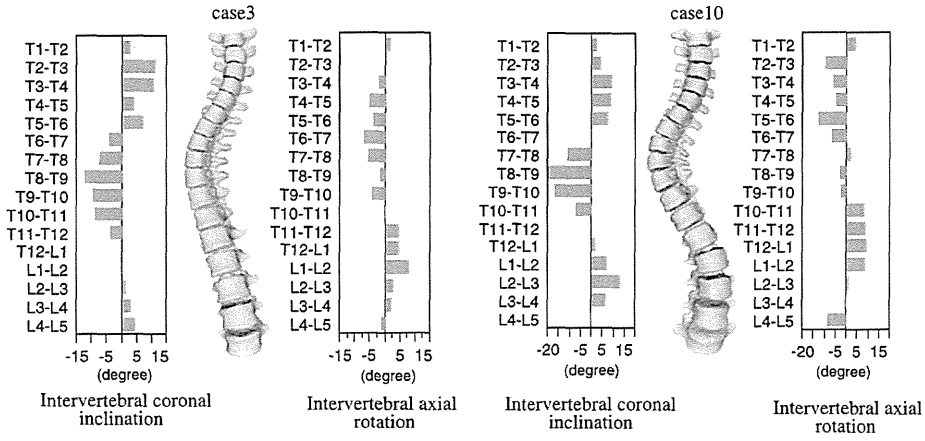

Fig. 4 Two representative cases. The bone models of both the thoracic and lumbar spine are shown in the *center*, and the *left sided graph* represents the intervertebral inclination angle in the coronal plane; the *right sided graph* represents the intervertebral rotational angle in the axial plane. *Left* case 3, *Right* case 10

in patients with AIS have been performed [8, 9, 21–23]. As morphometric studies, Parents et al. [21–23] created a 3D reconstruction of a large number of cadaveric bones, and compared normal vertebrae with the vertebrae of AIS. For example, vertebral wedging increased progressively toward the apex and pedicles located on the concavity were found to be significantly thinner than normal specimens [21–23]. In addition, the evaluation of global 3D correction between pre- and post-operative spinal 3D shape was also reported by Kadoury et al. [8, 9]. They reconstructed 3D models using bi-planar radiographs, and examined the difference among four operative methods. Steib et al. also performed 3D studies about the 3D change before and after surgical correction by in situ contouring technique using the reconstructed 3D models from bi-planar radiographs [6, 7, 16, 27]. However, these methods lacked accuracy since their method required only about 6–20 landmarks when reconstructing the bone models. Although an accurate assessment of 3D intervertebral deviation is crucial to the better surgical correction of the deformity, no detailed 3D study using an in vivo model of AIS has been reported.

Our results indicate the different deviation patterns between the intervertebral coronal plane deformity and intervertebral axial plane rotation. The intervertebral deformity in the coronal plane was larger near the apical region and smaller near the junctional region. Conversely, the intervertebral rotation in the axial plane was smaller near the apical region and larger near the junctional region. In 1994, Dubousset also showed that the intervertebral axial rotation reached its maximum at the extremities and its minimum at the apex [5]. However, the simple finite element models of only one case were used in the study and it is not known how to measure the intervertebral deviation [5]. Therefore, using the precise 3D evaluation method, we can show that the change in the intervertebral inclination angle in the coronal plane increased toward the apical region and decreased toward the junctional region, and that the converse tendency was noted for the axial intervertebral rotational angle in AIS patients for the first time.

There is a limitation in our method. The bone models were constructed from CT images taken in the supine position. Troell et al. [28] examined the radiographs of 287 girls with AIS and found that their mean Cobb angle, measured at standing position, was approximately 9° larger than that in the supine position, and the difference was 45° in the maximum. Yazici et al. [29] also showed that the average Cobb angle on a standing radiograph was approximately 16° larger than that in the supine position and they found that a rotational angle of 22.75° on the standing radiograph and 16.78° in the supine position. However, our results compared coronal with axial deviation under the same condition as supine. Though it is conceivable that the degree of the spinal deformity may be small in the supine position, it would appear that the features obtained from our study are not different from those obtained in the standing position.

The results in the present study can be applied to the surgical correction of AIS. The concave rod rotation maneuver, introduced by Cotrel and Dubousset, is generally concluded with derotation vertebral procedures. It's well accepted that rotation of precontoured concave rod (counter-clockwise) by alone has poor rotation improvement [1, 12–14, 17, 26]. Moreover, Kadoury et al. concluded that scoliosis also involves transverse plane rotation of the vertebrae in the opposite direction. In order to derotate the vertebrae, moments in the opposite sense should also be applied to the vertebrae [9]. According to our result, it might be easier to correct the rotation of each vertebra from the end vertebra to the apex using direct vertebral rotation technique.

Conclusion

We propose a new local coordinate system for deformed vertebrae of AIS. By using this coordinate system, the 3D intervertebral deviation in the coronal, axial and sagittal planes were measured. We found that the intervertebral deformity in the coronal plane was larger near the apical region and smaller near the junctional region. Conversely, the intervertebral rotation in the axial plane was smaller near the apical region and larger near the junctional region.

Conflict of interest None.

References

1. Asghar J, Samdani AF, Pahys JM, D'andrea LP, Guille JT, Clements DH, Betz RR (2009) Computed tomography evaluation of rotation correction in adolescent idiopathic scoliosis: a comparison of an all pedicle screw construct versus a hook-rod system. Spine 34:804–807
2. Benameur S, Mignotte M, Parent S, Labelle H, Skalli W, Guise J (2002) 3D biplanar statistical reconstruction of scoliotic vertebrae. Stud Health Technol Inform 91:281–285
3. Carpineta L, Labelle H (2003) Evidence of three-dimensional variability in scoliotic curves. Clin Orthop Relat Res 412:139–148
4. Cruickshank JL, Koike M, Dickson RA (1989) Curve patterns in idiopathic scoliosis. A clinical and radiographic study. J Bone Joint Surg [Br] 71:259–263
5. Dubousset J (1994) Three-dimensional analysis of the scoliotic deformity. In: Weinstein SL (ed) The pediatric Spine: Principles and Practices. Raven Press, New York, pp 479–496
6. Dumas R, Mitton D, Laporte S, Dubousset J, Steib JP, Lavaste F, Skalli W (2003) Explicit calibration method and specific device designed for stereoradiography. J Biomech 36:827–834
7. Dumas R, Steib JP, Mitton D, Lavaste F, Skalli W (2003) Three-dimensional quantitative segmental analysis of scoliosis corrected by the in situ contouring technique. Spine 28:1158–1162
8. Kadoury S, Cheriet F, Laporte C, Labelle H (2007) A versatile 3D reconstruction system of the spine and pelvis for clinical assessment of spinal deformities. Med Bio Eng Comput 45:591–602
9. Kadoury S, Cheriet F, Beauséjour M, Stokes IA, Parent S, Labelle H (2009) A three-dimensional retrospective analysis of the evolution of spinal instrumentation for the correction of adolescent idiopathic scoliosis. Eur Spine J 18:23–37
10. Kotwicki T, Napiontek M (2008) Intravertebral deformation in idiopathic scoliosis a transverse plane computer tomographic study. J Pediatr Orthop 28:225–229
11. King HA, Moe JH, Bradford DS, Winter RB (1983) The selection of fusion levels in thoracic idiopathic scoliosis. J Bone Joint Surg Am 65:1302–1313
12. Labelle H, Dansereau J, Bellefleur C, de Guise J, Rivard CH, Poitras B (1995) Peroperative three-dimensional correction of idiopathic scoliosis with the Cotrel–Dubousset procedure. Spine 15:1406–1409
13. Lenke LG, Bridwell KH, Baldus C, Blanke K, Schoenecker PL (1992) Cotrel–Dubousset instrumentation for adolescent idiopathic scoliosis. J Bone Joint Surg Am 74:1056–1067
14. Lenke LG, Bridwell KH, O'Brien MF, Baldus C, Blanke K (1994) Recognition and treatment of the proximal thoracic curve in adolescent idiopathic scoliosis with Cotrel–Dubousset instrumentation. Spine 15:1589–1597
15. Little DG, Sussman MD (1994) The Risser sign: a critical analysis. J Pediatr Orthop 14:569–575
16. Mitton D, Landry C, Véron S, Skalli W, Lavaste F, Guise JA (2000) 3D reconstruction method from biplanar radiography using non-stereocorresponding points and elastic deformable meshes. Med Biol Eng Comp 38:133–139
17. Moens P, Vanden Berqhe L, Fabry G, Bellemans J (1995) The Cortel–Dubousset device: prospective study on derotation. Rev Chir Orthop Reparatrice Appar Mot 81:428–432
18. Modi HN, Suh SW, Song HR, Lee SH, Yang JH (2008) Differential wedging vertebral body and intervertebral disc in thoracic and lumbar spine in adolescent idiopathic scoliosis—a cross sectional study in 150 patients. Scoliosis 3:11
19. Nash CL, Moe JH (1969) A study of vertebral rotation. J Bone Joint Surg Am 54:223–229
20. Oka K, Moritomo H, Murase T, Goto A, Sugamoto K, Yoshikawa H (2005) Patterns of carpal deformity in scaphoid nonunion: a 3-dimensional and quantitative analysis. J Hand Surg [Am] 30:1136–1144
21. Parent S, Labelle H, Skalli W, Latimer B, Guise J (2002) Morphometric analysis of anatomic scoliotic specimens. Spine 27:2305–2311
22. Parent S, Labelle H, Skalli W, Guise J (2004) Thoracic pedicle morphometry in vertebrae from scoliotic spines. Spine 29:239–248
23. Parent S, Labelle H, Skalli W, Guise J (2004) Vertebral wedging characteristic changes in scoliotic spines. Spine 29:E455–E462
24. Perdriolle R (1979) *La* scoliose: *Son* e'tude Tridimensionnelle. Ed. Maloine, Paris
25. Perdriolle R, Vidal J (1987) Morphology of scoliosis three-dimensional evolution. Orthopedics 10:909–915
26. Sawatzky BJ, Tredwell SJ, Jang SB, Black AH (1998) Effects of three-dimensional assessment on surgical correction and on hook strategies in multi-hook instrumentation for adolescent idiopathic scoliosis. Spine 23:201–205
27. Steib JP, Dumas R, Mitton D, Skalli W (2004) Surgical correction of scoliosis by in situ contouring: a detorsion analysis. Spine 29:193–199
28. Torell G, Nachemson A, Haderspeck-Grib K, Schultz A (1985) Standing and supine Cobb measures in girls with idiopathic scoliosis. Spine 10:425–427
29. Yazici M, Acaroglu ER, Alanay A, Deviren V, Cila A, Surat A (2001) Measurement of vertebral rotation in standing versus supine position in adolescent idiopathic scoliosis. J Pediatr Orthop 21:252–256

Three-dimensional kinematic estimation of mobile-bearing total knee arthroplasty from X-ray fluoroscopic images

Takaharu Yamazaki*[a], Kazuma Futai[b], Tetsuya Tomita[b], Yoshinobu Sato[c], Hideki Yoshikawa[d], Shinichi Tamura[a], Kazuomi Sugamoto[b]
[a]The Center for Advanced Medical Engineering and Informatics, Osaka University
[b]Division of Orthopaedic Biomaterial Science, Osaka University Graduate School of Medicine
[c]Department of Radiology, Osaka University Graduate School of Medicine
[d]Department of Orthopaedics, Osaka University Graduate School of Medicine

ABSTRACT

To achieve 3D kinematic analysis of total knee arthroplasty (TKA), 2D/3D registration techniques, which use X-ray fluoroscopic images and computer-aided design (CAD) model of the knee implant, have attracted attention in recent years. These techniques could provide information regarding the movement of radiopaque femoral and tibial components but could not provide information of radiolucent polyethylene insert, because the insert silhouette on X-ray image did not appear clearly. Therefore, it was difficult to obtain 3D kinematics of polyethylene insert, particularly mobile-bearing insert that move on the tibial component. This study presents a technique and the accuracy for 3D kinematic analysis of mobile-bearing insert in TKA using X-ray fluoroscopy, and finally performs clinical applications. For a 3D pose estimation technique of the mobile-bearing insert in TKA using X-ray fluoroscopy, tantalum beads and CAD model with its beads are utilized, and the 3D pose of the insert model is estimated using a feature-based 2D/3D registration technique. In order to validate the accuracy of the present technique, experiments including computer simulation test were performed. The results showed the pose estimation accuracy was sufficient for analyzing mobile-bearing TKA kinematics (the RMS error: about 1.0 mm, 1.0 degree). In the clinical applications, seven patients with mobile-bearing TKA in deep knee bending motion were studied and analyzed. Consequently, present technique enables us to better understand mobile-bearing TKA kinematics, and this type of evaluation was thought to be helpful for improving implant design and optimizing TKA surgical techniques.

Keywords: Total knee arthroplasty, Mobile-bearing insert, 3D kinematics, Accuracy validation, X-ray fluoroscopy, 2D/3D registration technique, Clinical applications

1. INTRODUCTION

In orthopaedics, total knee arthroplasty (TKA) is an effective treatment for functional disability and arthritic knees in which articular cartilage is damaged. TKA implants generally consist of metallic femoral and tibial components and a polyethylene bearing insert between them (Figure 1). The polyethylene insert replaces the damaged cartilage of the tibial plateau and provides a low-friction surface for the metallic implant component.

Quantitative assessment of three-dimensional (3D) kinematics of TKA is highly important for evaluating the outcome of surgical procedures and for improving the implants design and clinical outcome. To achieve 3D kinematic analysis of TKA, 2D/3D registration techniques, which use X-ray fluoroscopic images and computer-aided design (CAD) model of the knee implant, have attracted attention in recent years [1-4]. These studies could provide information regarding the movement of radiopaque femoral and tibial components but could not provide information of radiolucent polyethylene insert, because the insert silhouette on X-ray image did not appear clearly. Therefore, it was difficult to obtain 3D kinematics of polyethylene insert, particularly mobile-bearing insert that move on the tibial component.

Only a few studies have reported 3D kinematics of mobile-bearing insert in TKA using a fiducial markers technique based on X-ray images [5,6]. These studies are thought to be useful for 3D determination of the mobile-bearing insert kinematics. However, there is concern that the 3D pose estimation accuracy of the insert can be influenced by positional error of fiducial markers for the insert and projection number of makers on X-ray image. In previous studies, the pose estimation accuracy of the mobile-bearing insert has not been investigated, and therefore did not give assurance the same

Medical Imaging 2011: Image Processing, edited by Benoit M. Dawant, David R. Haynor,
Proc. of SPIE Vol. 7962, 79624B · © 2011 SPIE · CCC code: 1605-7422/11/$18 · doi: 10.1117/12.877815

degree of accuracy as femoral and tibial components. This study presents a technique and the accuracy for 3D kinematic analysis of mobile-bearing insert in TKA using X-ray fluoroscopy. The results of accuracy validation define the capabilities and limitations of 3D kinematic analysis of the insert. We also apply the technique to TKA patients during dynamic motion.

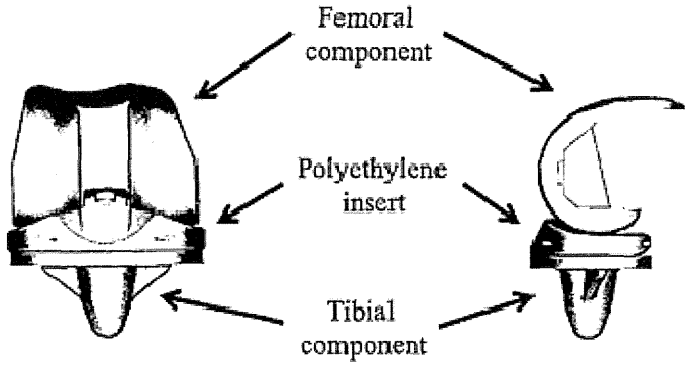

Figure 1. CAD models for femoral and tibial components and a polyethylene insert between them.

2. METHODS

2.1 Condition and requirement

To achieve 3D pose estimation of knee implants using X-ray fluoroscopy, it is necessary to know the parameters of the X-ray imaging system. The parameters of the imaging system are determined with a 3D calibration cube. The calibration cube has evenly spaced 217 metallic markers, which are employed as calibration markers. First, the calibration cube is placed in the viewing area of the imaging system and X-ray images are acquired. Next, because the X-ray images exhibit significant distortion introduced by image intensifiers, images are corrected with a non-linear distortion correction method. Finally, parameters of the imaging system (principal point and principal distance) are determined from 2D data (positions of the center of projected makers) on the corrected X-ray images and the known 3D data (positions and orientation) of the calibration cube with a non-linear calibration technique [7]. The principal point is the location on the image plane perpendicular to the incident X-ray, and the principal distance is the distance from the X-ray focus to the principal point.

In *vivo* knee motion after TKA was recorded as a series of digital X-ray images (1024x1024 pixels; 12 bits; 7.5 frames/sec) using a 12-inch digital image intensifier system (C-vision PRO-T, Shimadzu, Japan). Tests were typically performed using X-ray parameters of 70 kV, 400 mA and 1.2-2.0 ms duration, enabling nearly blur-free imaging of motion with higher per-frame exposure and image quality than in standard video-fluoroscopy.

2.2 Pose estimation of femoral and tibial components

For the 3D pose estimation of femoral and tibial components using X-ray fluoroscopy, a contour-based (feature-based) 2D/3D registration technique is utilized [2,4]. This technique uses implants silhouette contours on X-ray fluoroscopic images and CAD model of implants. The basic concept of this registration algorithm is that the 3D pose of a model can be determined by projecting rays from contour points in an image back to the X-ray focus, and noting that all of these rays are tangential to the model surface (Figure 2). The tangent condition therefore corresponds, in practice, to the minimum distance condition between the projection rays and the model surface. Then, a cost function E is defined as the sum of Euclidean distance d_i from point q_i on the projection rays (corresponding to the point p_i on the contours) to the closest point s_i on the CAD model surface.